Orientational Order of Molecular Assemblies on Rough Surfaces

Hannes C. Schniepp, Ho C. Shum, Dudley A. Saville,† and Ilhan A. Aksay*

Department of Chemical Engineering, Princeton University, Princeton, New Jersey 08544

Received: April 29, 2008

Using atomic force microscopy, we show that previous observations on the orientational order of micelles on atomically smooth crystals with directions dictated by the crystal symmetry is only valid for the case of perfectly smooth crystals. On rough surfaces, orientations are independent of the lattice symmetry and the observed directions can be explained by considering the guiding influence of topographic surface features.

Introduction

Surfactant aggregates exhibit strong, lattice-induced orientational order on a number of atomically smooth, crystalline substrates.[1−4] There have been several earlier attempts to rationalize this order. Manne and Gaub suspected a crystalline anisotropy in the van der Waals interactions as its origin.[2] Wanless and Ducker, in contrast, suggested that all observed orientational order is induced by topographic steps.[5] The latter view is not in agreement with a substantial amount of the reported experimental evidence: the great majority of surfactant micelles on highly oriented pyrolytic graphite (HOPG) surfaces run perpendicularly with respect to the lattice symmetry axes,[1,4] whereas the steps on cleaved HOPG are often unrelated to these axes.[6] Burgess and co-workers, finally, conducted liquid-cell scanning tunneling microscopy studies of surfactants on Au(111) surfaces at elevated electrical potentials.[7] They found flat monolayers of surfactant molecules epitactically grown on Au(111) and concluded that the orientation of surfactant micelles which are found at uncontrolled potentials is templated by such a flat surfactant layer. However, there is no direct evidence that the first layer of surfactant molecules in surfactant micelles exhibits such a crystalline order.

To understand the phenomenon of ordered surfactant adsorption in detail, it is desirable to perform fully atomic molecular dynamics simulations, taking into account electrostatic, hydrophobic, and van der Waals interactions between the substrate, the surfactant, and the solvent. So far, however, a satisfactory computational method has not been demonstrated for a system large enough to exhibit the micelle formation and orientation.[8−10] To treat the same system at the micellar (colloidal) length scale with a simpler approach, we recently chose to view a micelle as a macroscopic "rod" and have shown that anisotropic van der Waals torque between rod-like surfactant micelles and a graphite substrate is large enough to orient the micelles perpendicular to the symmetry axes of the graphite lattice.[11,12] In more recent experiments, we also studied the aggregates of sodium dodecyl sulfate (SDS) on Au(111), a system that is well-known[7,13] to recognize the lattice symmetry axes. When we introduced topography variations to these substrates, we found micelles in orientations unrelated to the gold symmetry axes suggesting that there are other mechanisms determining the orientation of surfactant admicelles, capable of overriding the lattice-induced van der Waals anisotropy.[13]

In order to understand the conditions leading to this transition from the lattice-induced orientational order to topography-induced orientational order, in this paper, we use single-atomic steps as model topographic features and demonstrate that the atomic steps are indeed capable of orienting surfactant micelles. Our results reveal a competition between lattice-induced and topography-induced orientational order. Based on these micellar-resolution images we show that the relative strength of these two mechanisms depends on the surfactant/substrate combination.

Our previous experiments have shown that surfactant surface populations are dynamic,[11] and that they are able to recover in response to external perturbations within milliseconds in a self-healing way.[14] This suggests that we are observing the propagation of such systems into a low-energy state (thermodynamic equilibrium). On inhomogeneous surfaces, the energy related to the adsorption of any species depends on the adsorption site. The total energy of the system is thus a function of the spatial conformation of the adsorbed species, in our case the morphology of the micellar surfactant adlayer. Kossel[15] and Stranski[16] were able to explain crystal growth and the observed crystal shapes by considering site-dependent adsorption energies. They calculated the adsorption energies for adding one more salt ion to specific sites such as kinks, ledges, and terraces of perfect salt crystals. They found that the adsorption at kinks is more favorable than at ledges and much more favorable than adsorption on terraces, as the number of available atomic partners providing attractive interactions decreases in that order.[15,16] This approach can be generalized to consider surface adsorption of objects of different kind and size.[17]

The great technological relevance of this site-dependent adsorption mechanism stems from the fact that topologically deterministic adsorption sites can guide self-assembly and induce order in systems that are difficult to control otherwise. The concept of employing topographical textures to guide adsorption and self-assembly has been demonstrated for a great variety of systems from atomic to micron length scales ("graphoepitaxy"[18]), including semiconductor[18−32] and metal[33−38] atoms, simple salts,[39] oxides,[40] proteins,[41] liquid crystals,[42] carbon nanotubes,[43,44] block copolymer domains,[45,46] organic electronic structures,[47,48] and colloids.[49] The orientation of block copolymer domains has also been controlled using chemical surface patterns in a similar way.[50−53] Furthermore, structures assembled by such techniques have been used as masks to produce quantum dot arrays,[54] memory storage devices,[55] nanowires,[56] magnetic storage media,[57] and silicon capacitors.[58] We demonstrate

* To whom correspondence should be addressed. E-mail: iaksay@princeton.edu.
† Deceased.

10.1021/jp805987b CCC: $40.75
Published on Web 08/27/2008

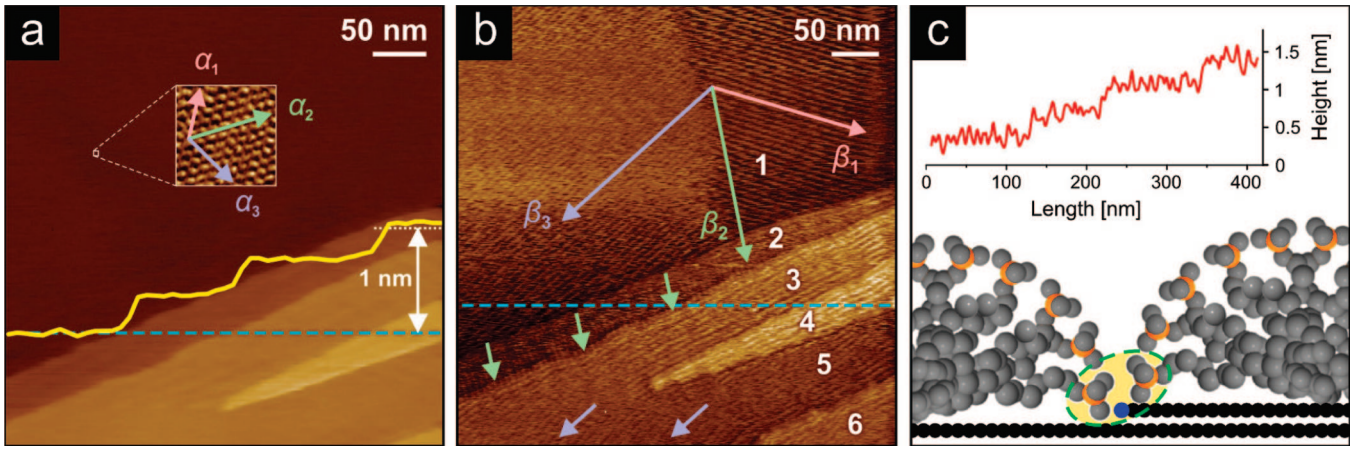

Figure 1. (a) High-force AFM topography image of graphite in 10 mM C_{16}TAC, showing the substrate. The yellow topography cross-section follows the light blue, dashed line and features single-atomic steps. The high-resolution inset shows the graphite lattice orientation with symmetry axes $\alpha_1/\alpha_2/\alpha_3$. (b) Imaging the same system at low force reveals the surface micelles with preferred orientations $\beta_1/\beta_2/\beta_3$. White numbers: terrace areas, separated by ledges. (c) Top: topography cross-section following the light blue, dashed line in (b), showing the topography modulation on the terraces due to micelle coverage. Bottom: schematic of two hemicylindrical micelles at a topographic step (gray and black atoms: carbon, orange atoms: nitrogen). Highlighted area: interaction zone between a step and the adjacent head groups.

graphoepitaxy at single-atomic steps, the smallest possible topographic features in single-crystalline substrates. Our study also shows that in case of surfactant micelles, graphoepitaxy is in competition with the lattice-induced orientation.

Experimental Section

Preparation of Samples and Solutions. Atomically smooth graphite surfaces were obtained by cleaving HOPG (SPI supplies, West Chester, PA) directly before the experiments. Gold surfaces were prepared by evaporating a 100 nm-thick gold film directly onto unheated, freshly cleaved mica substrates (without using any adhesion-providing intermediate metal layer). This was accomplished using a Denton V-502A (Denton Vacuum, Moorestown, NJ) electron beam evaporator at pressures below 10^{-6} mbar and a deposition rate of 0.3 nm/s. To obtain atomically smooth gold surfaces, these samples were annealed in a hydrogen flame, using a National 3H stainless steel hydrogen torch with an OX-3 tip (Premier Industries, Blaine, MN). The hydrogen pressure was 400 mbar and the torch regulator was adjusted to yield a flame about 7 cm long. The mica sheets were held in the flame for about 10 s at a distance of about 5 cm of the torch tip. We confirmed that the (111) planes were oriented parallel to the substrate surface by X-ray diffraction (XRD) characterization (see Supporting Information) and atomic-resolution lattice scans obtained by atomic force microscopy (AFM). The annealed samples were used within minutes after the annealing process to reduce contamination from air.

Solutions of hexadecyltrimethylammonium bromide (C_{16}TAB) were prepared by dissolving C_{16}TAB powder (99% grade, Sigma-Aldrich, St. Louis, MO) in water deionized using a Picopure 2 UV Plus system (Hydro Service and Supplies, Inc., Durham, NC), featuring a resistivity of 18 MΩ cm. Solutions of C_{16}TAC were obtained by diluting a 25 wt % aqueous C_{16}TAC solution ("purum" grade, Sigma-Aldrich) with deionized water. SDS solutions were prepared from SDS ("Bio-Chemika Ultra" grade ≥99% (GC), Fluka, Buchs, Switzerland). The pH values of the surfactant solutions were not further adjusted.

Atomic Force Microscopy (AFM). All images were acquired in liquid environment using a commercial MultiMode AFM (Veeco, Santa Barbara, CA) with a NanoScope IIIa controller (software version v5.12r5), equipped with an FC type contact-mode liquid cell. Two types of AFM probes were used: (i) NP-S type (Veeco) oxide-sharpened silicon nitride tips with reflective gold coating on the back side and a nominal spring constant and tip radius of curvature of $k = 0.06$ N/m and $r = 20$ nm, respectively, and (ii) PointProbe Plus PPP-BSI (Nanosensors, Neuchatel, Switzerland) uncoated silicon cantilevers ($r < 7$ nm, $k = 0.05$ N/m). The probes were cleaned in an ozone chamber (UVOCS, Montgomeryville, PA) for 60 min prior to the experiment. The studies of SDS on smooth and rough gold were conducted using the PPP-BSI tips. The NP-S probes were used in all other experiments. The fluid cell (volume: 0.5 mL) was flushed with 5 mL of deionized water and left for one hour to reach thermal equilibrium. Surfactant solutions were then added and imaging started.

All imaging was performed in static mode using different force set points and line frequencies of 2−7 Hz. The highest possible integral and proportional gains (typically ∼5) were used to obtain the most accurate representation of the sample. Imaging of micellar aggregates was performed at low force set points, in the precontact regime (previously described as "double-layer repulsion"[1,59] or "soft contact"[60] imaging modes).

Results and Discussion

The result of liquid-cell AFM at the interface of a graphite(0001) surface and a 10 mM C_{16}TAC solution is shown in Figure 1. Figure 1a shows an image obtained with a high[14,61] vertical force, such that the tip established direct contact with the graphite substrate. This is proven by the high-resolution scan revealing the graphite lattice (top inset, lattice symmetry axes $\alpha_1/\alpha_2/\alpha_3$ highlighted by pink/mint green/violet arrows, respectively). The top half of Figure 1a is virtually defect free, whereas the bottom half shows several single-atomic steps on the surface. The topography section across three of those steps following the light blue, dashed line shows that the observed step height is in agreement with the expected[62] 0.34 nm d_{0002} spacing of graphite. The direction of this cross-section was chosen strictly parallel to the fast scanning direction in order to minimize inaccuracy due to drift and piezo creep. Figure 1b was taken at low[14,61] force and visualizes the C_{16}TAC surface micelles, which are known to be of hemicylindrical morphology.[1−3] In agreement

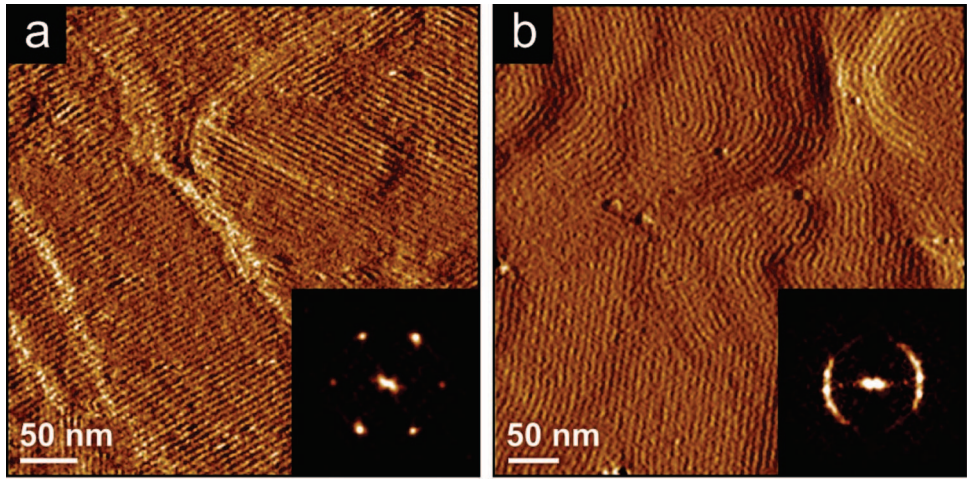

Figure 2. Chemistry dependence of orientational order on flame-annealed Au(111): for very similar surfactants, either the substrate lattice (10 mM C_{16}TAC, panel (a)) or the substrate topography features (10 mM C_{16}TAB, panel (b)) determine the micelle orientation.

with previous reports, [1−3,11,12] on the majority of the surface, the micelles are oriented in directions $\beta_1/\beta_2/\beta_3$, perpendicularly with respect to the $\alpha_1/\alpha_2/\alpha_3$ lattice directions. However, we observe that not all micelles are oriented according to this previously reported rule. In the vicinity of the topographic steps on the graphite substrate, some micelles are oriented parallel to these steps at an angle of about 15° with respect to the usually preferred β_3 direction. Using topography cross-sections we determined that these micelles had the same height as micelles further away from the step. A typical topography section across several of the micelle-covered HOPG steps following the light blue, dashed line is shown in Figure 1c, top. The obtained profile is very similar to the one shown in Figure 1a, except the topography is now periodically modulated by the micelle population with an amplitude of about 0.2 nm. This means that within the precision of the measurement (∼0.1 nm) all surface micelles have identical heights. It is thus safe to assume that the micelles in the vicinity of topographic steps of the substrate are hemicylindrical, as well. If they were full cylindrical micelles, they would have been easily detected, as they should be ∼2 nm higher than hemicylindrical ones.

Our interpretation of this orientational alignment with the atomic step is that when a hemicylindrical micelle runs parallel to a step, the bottom layer of the constituting surfactant molecules must be predominantly oriented perpendicular to the step as sketched in Figure 1c (bottom). For the preferred adsorption of the micelle at an orientation along the step, we suspect electrostatic forces. The ledges in graphite (black) tend to acquire negative charge through the formation of carboxylic groups (schematically represented through a blue atom in Figure 1c),[63,64] leading to an attraction of the cationic trimethylammonium surfactant head groups (nitrogen atoms shown in orange, carbon atoms shown in gray color). This specific interaction may be the reason that we see orientation even though the height of the hemicylindrical surfactant micelles (∼2 nm) is about an order of magnitude larger than the step height (∼0.34 nm). For polymer nanodomains, in contrast, it was reported that alignment is only achieved for step heights of the same size than the domains; when the step size was reduced by 50% alignment was absent.[45] In addition to offering electrostatic attraction, the steps may also represent sites with increased van der Waals interactions, since guest molecules located at the step can achieve simultaneous proximity with atoms of bottom and top substrate layers. This would be analogous to the original model of Kossel[15] and Stranski,[16] rationalizing atomic ledges and kinks as sites of increased adsorption energy. To evaluate the relative importance of electrostatic van der Waals forces for orientation, similar experiments using nonionic surfactants may be beneficial.

It is worth performing a deeper analysis of Figure 1b, where we have denoted 6 terrace areas by white numbers that are separated by single-atomic steps. In areas 2−6, we observe alignment of the micelles with the steps, while alignment in area 1 is very weak. A likely explanation is that areas 2−6 are relatively narrow (20−80 nm), so that each micelle in one of these areas has two steps in its vicinity contributing to the alignment. Running parallel to the steps in areas 2−6 allows for long, straight micelles (200−300 nm), whereas orientation along the β_3 direction, for instance, would require to break micelles up into shorter pieces. This indicates that the energetic cost of breaking up a micelle is considerable. On area 5, which is relatively wide, we observe that the orientation of the micelles now has a strong tendency to deviate from the step direction. To the left of area 4, where areas 3 and 5 merge, finally, we observe that the micelles bend and follow the β_3 direction, indicated by small violet arrows in Figure 1b. This observation can be generalized: the energy associated with (i) orientation in registry with the substrate lattice is proportional to the area, whereas the energies associated with (ii) alignment along a step, (iii) bending or (iv) breaking up micelles are proportional to the linear dimension of the topographic step. It is thus expected that (i) is dominant on larger terraces, whereas (ii)−(iv) become more important on smaller terraces.

A similar analysis can be performed for other surfactant/substrate combinations. For C_{16}TAC on Au(111), we have shown[61] that the surfactant micelles strictly align perpendicular to the gold lattice in a very similar way as on graphite, as shown in Figure 2a and its Fourier transform in the inset. We hardly see micelles lining up with topographic steps in this case; some of the micelles run across topographic steps of the substrate. For cetyltrimethylammonium bromide C_{16}TAB on Au(111), in contrast, an ordering influence of the lattice is not detectable,[61,65] as shown in Figure 2b and its Fourier transform in the inset. The micelles follow the topographic features, for instance at the circular structure on the top right of the image, undergoing a significant amount of bending.[61] The step-induced orientation persists even several micelle diameters away from the steps, suggesting that (i) their ordering influence is particularly strong in the C_{16}TAB/Au(111) system, and (ii) that the lattice-induced ordering, and (iii) the restoring forces due to micelle bending

are relatively weak. Jaschke et al.[65] have suggested that the alignment at the topographic steps is due to specific adsorption of Br^- ions at these sites. It is currently unclear why the lattice-induced anisotropy is absent for $C_{16}TAB$. Both Cl^- and Br^- ions are known to adsorb on Au(111) and form close-packed hexagonal layers.[66] One significant difference between the two ionic species is that only the former shows angular alignment with the gold lattice, whereas the latter adsorbs at random orientations. [66] The Br^- ions may thus annihilate the ordering influence of the gold lattice. Moreover, it is possible that the aggregates of $C_{16}TAB$ vs $C_{16}TAC$ are of different morphology. For $C_{16}TAB$, Jaschke et al. have suggested that chemisorption of the Br^- counterions causes negative charging of the gold substrate,[65] leading to full-cylindrical micelles where the surfactant head groups are facing the substrate. In contrast, Cl^- ions are known to adsorb on Au(111) in smaller amounts than Br^- at a given potential[67−69] and thus induce a negative surface charge of smaller magnitude. The interaction between $C_{16}TAC$ and Au(111) may therefore not be dominated by electrostatic forces and feature a hemicylindrical aggregate morphology instead, with the surfactant tail groups contacting the substrate. As a matter of fact, hemicylindrical micelles have been suggested for $C_{16}TAOH$.[65] This is in agreement with recent reports that $C_{16}TAC$ adsorbs in lower quantities on Au(111) than $C_{16}TAB$.[70] Previously, studies have shown that full-cylindrical surfactant surface micelles exhibit much less substrate-induced angular orientation than hemicylindrical micelles.[2]

Similar to $C_{16}TAC$, SDS exhibits preferred orientation of the adsorbed micelles on atomically smooth Au(111).[7,61,65] The low-force AFM topography image presented in Figure 3a shows a flame-annealed gold surface in contact with a 10 mM aqueous solution of SDS. The majority of the micelles are oriented in one of the three preferred directions (parallel to the yellow arrows). The exceptions are highlighted by light blue ellipses. In all these highlighted examples, the micelles follow the boundaries between areas of different substrate heights (represented in the image by different brightness/color). Although not directly visible in Figure 3a, we conjecture that atomic steps in the substrate account for these height differences, and that the expected step directions coincide with the observed orientations of the micelles. We thus conclude that SDS micelles are also subject to orientation at topographic steps on Au(111), overriding the lattice-induced orientation. Figure 3b shows the micelles adsorbed from a 10 mM SDS solution on the unannealed, rough gold surface. It features the typical "rolling hill" morphology[71] with a peak-to-peak topography of ~10 nm as shown by the topography profile (in yellow) along the light blue, dashed line of the inset. The substrate surface is purely Au(111) as determined by XRD analysis (see Supporting Information). Nevertheless, only a small minority of the surface micelles—highlighted by orange arrows—exhibits the linear, parallel morphology characteristic of micelles adsorbed on atomically flat Au(111). The topography profile of Figure 3b shows that micelles are linear and parallel only in flat areas where no or a few topographic steps are to be expected. The higher-magnification topography image presented in Figure 3c shows more clearly not only the flat areas populated by straight micelles (highlighted by yellow circles), but also the areas with significant topography, featuring micelle population of a more disordered morphology[13] (highlighted by light blue circles). Analyzing many AFM images similar to Figure 3b and c, we found 19 grains showing straight, parallel micelles of two or three different orientations on a single grain, as highlighted in Figure 3c by the arrows in the large yellow circle. In all cases these directions had relative angles of 120° ± 4°. From this, we conclude that on rough surfaces the orientation of straight micelles is also lattice-controlled. On even rougher samples, finally, there are no more apparent areas that exhibit straight and parallel micelles, as shown in the AFM deflection image of Figure 3d. Although these micellar structures first seem very disordered, a closer analysis reveals that, in many cases, the micelles are entwining around the gold grains, similar to the contour lines on a relief map (highlighted by orange arrows in Figure 3b and d). Since the atomic steps on a Au(111) surface represent lines of constant height, this observation is in line with our previously discussed finding that SDS micelles tend to align with topographic steps. Thus, we are able to rationalize the structural appearance of elongated SDS micelles on topography-rich gold surfaces: in areas with topographic changes, the micelle orientation is determined by surface steps; in flat areas orientational registry with the substrate lattice is enforced.

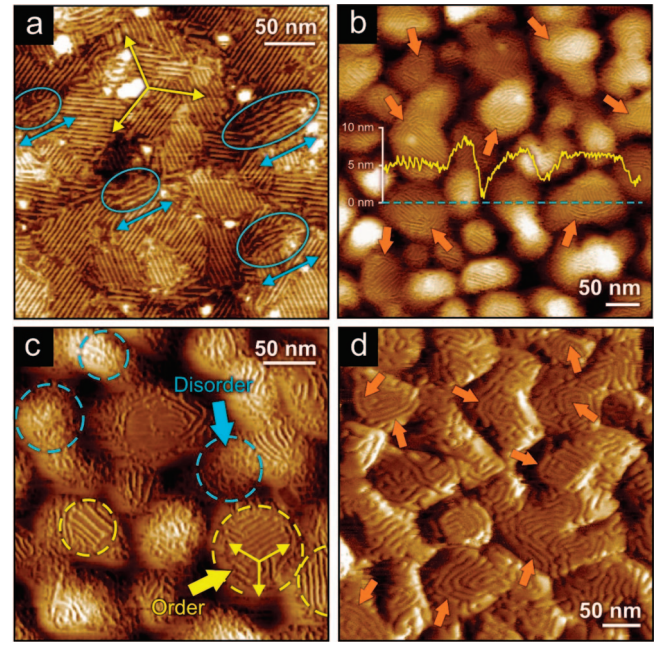

Figure 3. AFM images of gold surfaces in contact with a 10 mM SDS solution. (a) On large, flat areas the micelles are oriented in one of three preferred orientations (highlighted by yellow arrows). Only at topographic steps micelles exhibit orientations in different directions (highlighted by light blue arrows and ellipses). (b) On rougher surfaces only the flat areas show orientational order. Inset: substrate roughness visualized in cross-section following the dashed, light blue line. (c) Close-up of the sample shown in (b), revealing ordered (yellow) and disordered (light blue) areas. (d) On rougher substrates with smaller grain sizes, the micelles do not show preferred orientations. The orange arrows denote areas in which the micelles entwine around the grains (panels (b), (d)).

Conclusions

We have shown that the spatial conformation of micellar surfactant aggregates depends on not only the crystal symmetry but also on the topographic morphology of the substrate. On many defect free, crystalline surfaces, the surfactant micelles are oriented perpendicular with respect to the surface lattice symmetry axes. When topographic surface steps are present, oriented adsorption along such steps is preferred and overrides the lattice-induced orientation. For the case of the $C_{16}TAB$ micelles observed on Au(111), topography-induced orientation dominates the organization

of all micelles. In contrast, the organization of C_{16}TAC micelles on Au(111) seems to be strongly dominated by lattice-induced orientation. For C_{16}TAC on graphite and SDS on Au(111), we observe a competition between the two mechanisms. As demonstrated for the system SDS/Au(111), the observed micellar morphology depends strongly on the topography of the substrate: on an atomically flat substrate, perfect orientation perpendicular to the lattice symmetry axes can be observed; on a sample with feature-rich topography, the lattice-induced orientation can be completely overruled by topography-induced orientation.

Acknowledgment. We gratefully acknowledge the help of Michael J. Souza and Caroline M. Murira with flame-annealing and providing evaporated gold samples. Financial support from ARO/MURI under Grant No. W911NF-04-1-0170 and from the NASA University Research, Engineering, and Technology Institute on BioInspired Materials (BIMat) under Award No. NCC-1-02037 is greatly appreciated.

Supporting Information Available: Information on experimental methods and the XRD analysis of our gold substrates. This material is available free of charge via the Internet at http://pubs.acs.org.

References and Notes

(1) Manne, S.; Cleveland, J. P.; Gaub, H. E.; Stucky, G. D.; Hansma, P. K. *Langmuir* **1994**, *10*, 4409.
(2) Manne, S.; Gaub, H. E. *Science* **1995**, *270*, 1480.
(3) Wanless, E. J.; Ducker, W. A. *J. Phys. Chem.* **1996**, *100*, 3207.
(4) Aksay, I. A.; Trau, M.; Manne, S.; Honma, I.; Yao, N.; Zhou, L.; Fenter, P.; Eisenberger, P. M.; Gruner, S. M. *Science* **1996**, *273*, 892.
(5) Wanless, E. J.; Ducker, W. A. *Langmuir* **1997**, *13*, 1463.
(6) Chang, H.; Bard, A. J. *Langmuir* **1991**, *7*, 1143.
(7) Burgess, I.; Jeffrey, C. A.; Cai, X.; Szymanski, G.; Galus, Z.; Lipkowski, J. *Langmuir* **1999**, *15*, 2607.
(8) Shelley, J. C.; Shelley, M. Y. *Curr. Opin. Colloid In.* **2000**, *5*, 101.
(9) Sammalkorpi, M.; Karttunen, M.; Haataja, M. *J. Phys. Chem. B* **2007**, *111*, 11722.
(10) Sammalkorpi, M.; Panagiotopoulos, A. Z.; Haataja, M. *J. Phys. Chem. B* **2008**, *112*, 2915.
(11) Saville, D. A.; Chun, J.; Li, J.-L.; Schniepp, H. C.; Car, R.; Aksay, I. A. *Phys. Rev. Lett.* **2006**, *96*, 018301.
(12) Chun, J.; Li, J.-L.; Car, R.; Aksay, I. A.; Saville, D. A. *J. Phys. Chem. B* **2006**, *110*, 16624.
(13) Schniepp, H. C.; Shum, H. C.; Saville, D. A.; Aksay, I. A. *J. Phys. Chem. B* **2007**, *111*, 8708.
(14) Schniepp, H. C.; Saville, D. A.; Aksay, I. A. *J. Am. Chem. Soc.* **2006**, *128*, 12378.
(15) Kossel, W. *Nachr. Ges. Wiss. Göttingen* **1927**, 135.
(16) Stranski, I. N. *Z. Phys. Chem.-Stoch. Ve.* **1928**, *136*, 259.
(17) Givargizov, E. I. *Thin Solid Films* **1990**, *189*, 389.
(18) Geis, M. W.; Flanders, D. C.; Smith, H. I. *Appl. Phys. Lett.* **1979**, *35*, 71.
(19) Geis, M. W.; Flanders, D. C.; Smith, H. I.; Antoniadis, D. A. *J. Vac. Sci. Technol.* **1979**, *16*, 1640.
(20) Flanders, D. C. *J. Vac. Sci. Technol.* **1980**, *17*, 1195.
(21) Geis, M. W.; Antoniadis, D. A.; Silversmith, D. J.; Mountain, R. W.; Smith, H. I. *Appl. Phys. Lett.* **1980**, *37*, 454.
(22) Smith, H. I. *J. Am. Phys. Soc.* **1980**, *25*, 225.
(23) Geis, M. W.; Antoniadis, D. A.; Silversmith, D. J.; Mountain, R. W.; Smith, H. I. *Jpn. J. Appl. Phys* **1981**, *20*−*1*, 39.
(24) Geis, M. W.; Antoniadis, D. A.; Silversmith, D. J.; Mountain, R. W.; Smith, H. I. *J. Vac. Sci. Technol.* **1981**, *18*, 229.
(25) Mori, H. *Jpn. J. Appl. Phys* **1981**, *20*, L905.
(26) Smith, H. I.; Geis, M. W. *J. Electrochem. Soc.* **1982**, *129*, C100.
(27) Smith, H. I.; Thompson, C. V.; Geis, M. W.; Lemons, R. A.; Bosch, M. A. *J. Electrochem. Soc.* **1983**, *130*, 2050.
(28) Smith, H. I.; Thompson, C. V.; Atwater, H. A. *J. Cryst. Growth* **1983**, *65*, 337.
(29) Givargizov, E. I.; Limanov, A. B.; Zadorozhnaya, L. A.; Lazarenko, M. A.; Lukina, I. G. *J. Cryst. Growth* **1983**, *65*, 339.
(30) Sakano, K.; Moriwaki, K.; Aritome, H.; Namba, S. *Jpn. J. Appl. Phys., Part 2* **1982**, *21*, L636.
(31) Geis, M. W.; Tsaur, B. Y.; Flanders, D. C. *Appl. Phys. Lett.* **1982**, *41*, 526.
(32) Yonehara, T.; Smith, H. I.; Thompson, C. V.; Palmer, J. E. *Appl. Phys. Lett.* **1984**, *45*, 631.
(33) Darken, L. S.; Lowndes, D. H. *Appl. Phys. Lett.* **1982**, *40*, 954.
(34) Darken, L. S. *J. Electrochem. Soc.* **1983**, *130*, 1274.
(35) Klews, P. M.; Anton, R.; Harsdorff, M. *J. Cryst. Growth* **1985**, *71*, 491.
(36) Kushida, K.; Takeuchi, H.; Kobayashi, T.; Takagi, K. *Appl. Phys. Lett.* **1986**, *48*, 764.
(37) Klews, P. M.; Anton, R.; Harsdorff, M. *J. Vac. Sci. Technol., A* **1987**, *5*, 1931.
(38) Trolier, S.; Kushida, K.; Takeuchi, H. *J. Cryst. Growth* **1989**, *98*, 469.
(39) Smith, H. I.; Flanders, D. C. *Appl. Phys. Lett.* **1978**, *32*, 349.
(40) Klykov, V. I.; Gladkov, N. M. *Cryst. Res. Technol.* **1985**, *20*, K55.
(41) Givargizov, E. I.; Kliya, M. O.; Melikadamyan, V. R.; Grebenko, A. I.; Demattei, R. C.; Feigelson, R. S. *J. Cryst. Growth* **1991**, *112* 758.
(42) Flanders, D. C.; Shaver, D. C.; Smith, H. I. *Appl. Phys. Lett.* **1978**, *32*, 597.
(43) Ismach, A.; Kantorovich, D.; Joselevich, E. *J. Am. Chem. Soc.* **2006**, *127*, 11554.
(44) Ismach, A.; Joselevich, E. *Nano Lett.* **2006**, *6*, 1706.
(45) Segalman, R. A.; Yokoyama, H.; Kramer, E. J. *Adv. Mater.* **2001**, *13*, 1152.
(46) Hahn, J.; Webber, S. E. *Langmuir* **2003**, *19*, 3098.
(47) van de Craats, A. M.; Stutzmann, N.; Bunk, O.; Nielsen, M. M.; Watson, M.; Mullen, K.; Chanzy, H. D.; Sirringhaus, H.; Friend, R. H. *Adv. Mater.* **2003**, *15*, 495.
(48) Ikeda, S.; Saiki, K.; Tsutsui, K.; Edura, T.; Wada, Y.; Miyazoe, H.; Terashima, K.; Inaba, K.; Mitsunaga, T.; Shimada, T. *Appl. Phys. Lett.* **2006**, *88*, 251905.
(49) Deckman, H. W.; Dunsmuir, J. H.; Garoff, S.; McHenry, J. A.; Peiffer, D. G. *J. Vac. Sci. Technol., B* **1988**, *6*, 333.
(50) Kim, S. O.; Solak, H. H.; Stoykovich, M. P.; Ferrier, N. J.; de Pablo, J. J.; Nealey, P. F. *Nature* **2003**, *424*, 411.
(51) Stoykovich, M. P.; Muller, M.; Kim, S. O.; Solak, H. H.; Edwards, E. W.; de Pablo, J. J.; Nealey, P. F. *Science* **2005**, *308*, 1442.
(52) Chuang, V. P.; Cheng, J. Y.; Savas, T. A.; Ross, C. A. *Nano Lett.* **2006**, *6*, 2332.
(53) Edwards, E. W.; Muller, M.; Stoykovich, M. P.; Solak, H. H.; de Pablo, J. J.; Nealey, P. F. *Macromolecules* **2007**, *40*, 90.
(54) Park, M.; Harrison, C.; Chaikin, P. M.; Register, R. A.; Adamson, D. H. *Science* **1997**, *276*, 1401.
(55) Li, R. R.; Dapkus, P. D.; Thompson, M. E.; Jeong, W. G.; Harrison, C.; Chaikin, P. M.; Register, R. A.; Adamson, D. H. *Appl. Phys. Lett.* **2000**, *76*, 1689.
(56) Chai, J.; Wang, D.; Fan, X. N.; Buriak, J. M. *Nat. Nanotechnol.* **2007**, *2*, 500.
(57) Naito, K.; Hieda, H.; Sakurai, M.; Kamata, Y.; Asakawa, K. *IEEE Trans. Magn.* **2002**, *38*, 1949.
(58) Black, C. T. *Appl. Phys. Lett.* **2001**, *79*, 409.
(59) Senden, T. J.; Drummond, C. J.; Kekicheff, P. *Langmuir* **1994**, *10*, 358.
(60) Patrick, H. N.; Warr, G. G.; Manne, S.; Aksay, I. A. *Langmuir* **1997**, *13*, 4349.
(61) Schniepp, H. C.; Saville, D. A.; Aksay, I. A. *Langmuir* **2008**, *24*, 626.
(62) Kelly, B. T., *The Physics of Graphite*; Applied Science: Essex, England, 1981.
(63) Zoval, J. V.; Biernacki, P. R.; Penner, R. M. *Anal. Chem.* **1996**, *68*, 1585.
(64) Szabo, T.; Berkesi, O.; Forgo, P.; Josepovits, K.; Sanakis, Y.; Petridis, D.; Dekany, I. *Chem. Mater.* **2006**, *18*, 2740.
(65) Jaschke, M.; Butt, H.-J.; Gaub, H. E.; Manne, S. *Langmuir* **1997**, *13*, 1381.
(66) Magnussen, O. M.; Ocko, B. M.; Adzic, R. R.; Wang, J. X. *Phys. Rev. B* **1995**, *51*, 5510.
(67) Shi, Z. C.; Lipkowski, J. *J. Electroanal. Chem.* **1996**, *403*, 225.
(68) Shi, Z. C.; Lipkowski, J.; Mirwald, S.; Pettinger, B. *J. Chem. Soc., Faraday Trans.* **1996**, *92*, 3737.
(69) Lipkowski, J.; Shi, Z. C.; Chen, A. C.; Pettinger, B.; Bilger, C. *Electrochim. Acta* **1998**, *43*, 2875.
(70) Kawasaki, H.; Nishimura, K.; Arakawa, R. *J. Phys. Chem. C* **2007**, *111*, 2683.
(71) Chidsey, C. E. D.; Loiacono, D. N.; Sleator, T.; Nakahara, S. *Surf. Sci.* **1988**, *200*, 45.

JP805987B